Published in final edited form as:
Mol Imaging Biol. 2013 February ; 15(1): 40–47. doi:10.1007/s11307-012-0562-2.

Differentiation of Reactive and Tumor Metastatic Lymph Nodes with Diffusion-weighted and SPIO Enhanced MRI

Fan Zhang[1,2], **Lei Zhu**[1,2], **Xinglu Huang**[2], **Gang Niu**[2,*], and **Siouan Chen**[2,*]

[1]Center for Molecular Imaging and Translational Medicine, School of Public Health, Xiamen University, Xiamen 361000, China

[2]Laboratory of Molecular Imaging and Nanomedicine (LOMIN), National Institute of Biomedical Imaging and Bioengineering (NIBIB), National Institutes of Health (NIH), Bethesda, MD 20892, USA

Abstract

Objectives—Determination of lymphatic metastasis is of great importance for both treatment planning and patient prognosis. We aim to distinguish tumor metastatic lymph nodes (TLNs) and reactive lymph nodes (RLNs) with diffusion-weighted and superparamagnetic iron oxide (SPIO) enhanced magnetic resonance imaging (MRI).

Materials and methods—Ipsilateral popliteal lymph node metastasis or lymphadenitis model was established by hock injection of either luciferase-expressing 4T1 murine breast cancer cells or Complete Freund Adjuvant (CFA) in male Balb/C mice. At different time points after inoculation, bioluminescence imaging, T_2-weighted, diffusion-weighted and SPIO enhanced MRI were performed. Imaging findings were confirmed by histopathological staining.

Results—Size enlargement was observed in both TLNs and RLNs. At day 28, TLNs showed strong bioluminescence signal and bigger size than RLNs ($p < 0.01$). At early stages up to day 21, both TLNs and RLNs appeared homogeneous on diffusion-weighted imaging (DWI). At day 28, TLNs showed heterogeneous apparent diffusion coefficient (ADC) map with significantly higher average ADC value of $0.41 \pm 0.03 \times 10^{-3}$ mm^2/s than that of RLNs ($0.34 \pm 0.02\ 10^{-3}$ mm^2/s, $p < 0.05$). On SPIO enhanced MRI, both TLNs and RLNs showed distinct T_2 signal reduction at day 21 after inoculation. At day 28, TLNs demonstrated partial uptake of the iron oxide particles, which was confirmed by Prussian blue staining.

Conclusions—Both diffusion-weighted and SPIO enhanced MRI can distinguish tumor metastatic lymph nodes from reactive lymph nodes. However, neither method is able to detect tumor metastasis to the draining lymph nodes at early stages.

Keywords

Lymph node metastasis; diffusion-weighted imaging (DWI); superparamagnetic iron oxide (SPIO); magnetic resonance imaging (MRI); apparent diffusion coefficient (ADC) map

Introduction

Lymphatic metastasis is an important prognostic factor in patients with cancer. Determination of nodal status is also critical for appropriate treatment planning. Although

*Correspondence should be addressed to: Dr. Siouan Chen, shawn.chen@nih.gov; or Dr. Gang Niu, niug@mail.nih.gov.

Conflict of Interest Disclosure
The authors declare that they have no conflict of interest.

lymph nodes can be detected and visualized by several imaging modalities including ultrasound (US), computed tomography (CT) and magnetic resonance imaging (MRI), the differentiation between benign and malignant lymph nodes remains challenging [1, 2]. Enlarged reactive nodes are frequently present along the lymphatic drainage pathways, particularly of large and/or necrotic tumors, which may mimic lymph node metastasis [3].

Diffusion-weighted magnetic resonance imaging (DWI) has been intensively investigated in both preclinical models and patients with cancer for lymph node characterization [4–6]. DWI derives its contrast from the regional differences in the mobility of water molecules [7, 8]. By systematically increasing the strength of the gradient and measuring the decrease in observed ^{1}H signal intensity, the apparent diffusion coefficient (ADC) can be determined [9]. Due to the different cellular density and extracellular diffusion, metastatic lymph nodes may be distinguishable from normal lymph nodes with ADC measurements [10]. However, the discrepancy still exists between studies from different groups [11–13]. Sumi *et al.* [14] reported that metastatic lymph nodes have higher ADC values than lymph nodes without tumor metastasis while Razek *et al.* [11] and Eiber *et al.* [15] reported that metastatic lymph nodes have lower ADC values. Moreover, a longitudinal analysis of changes in lymph node volume and ADC in healthy, metastatic, and hyperplastic lymph nodes revealed that enlarged reactive or malignant nodes could not be differentiated based on their ADC values [5].

MRI with superparamagnetic iron oxide (SPIO) is also gaining acceptance as a non-invasive method for the detection of lymph node metastasis [16–20]. The underlying mechanism is that superparamagnetic nanoparticles are phagocytosed by reticuloendothelial cells in normal lymphoid tissues, but not in tumor tissue, because they lack reticuloendothelial cells. The nanoparticles induce a signal drop in lymphoid tissues on T_2-weighted images because of their superparamagnetic effect. Therefore, metastatic tumors can be differentiated from normal lymphoid tissues using SPIO-enhanced MRI [21].

In this study, we performed longitudinal DWI in both mouse lymph node metastasis and CFA (Complete Freund's Adjuvant) models [22]. With the same models, we also performed contrast enhanced MRI after interstitial injection of SPIO and tumor metastasis was further evaluated in tumor draining lymph nodes.

Materials and methods

Animal models

Luciferase-expressing 4T1 murine breast cancer cells were maintained at 37 °C in a humidified atmosphere containing 5% CO_2 in Dulbecco's Modification of Eagles Medium (DMEM) with 10% fetal bovine serum (FBS). The lymph node metastasis model was established in 4–6 week-old female BALB/c mice by hock injection of 0.5×10^{6} 4T1 cells to the right side. The reactive lymph node model was established in another group of mice by aseptic administration of 20 μl of CFA (Complete Freund's Adjuvant) to the left hock region. At day 7, 14, 21 and 28 after 4T1 cell inoculation or CFA injection, tumor bearing BALB/C mice and CFA injected BALB/C mice underwent bioluminescence imaging and MRI. Animal procedures were performed according to a protocol approved by the National Institutes of Health Clinical Center Animal Care and Use Committee (NIH CC/ACUC).

Imaging protocol

Multiple modality imaging was performed according to the protocol described in Table 1. At each time point, BLI was performed immediately before MRI scan. Among them, 5 mice in each group underwent longitudinal DWI MRI for four times and lymph nodes samples were collected after the last MRI scan at day 28. SPIO enhanced MRI was perform at either day

21 or day 28. Lymph nodes sampling was performed immediately after imaging for histopathological examination.

Bioluminescence Imaging

Tumor metastatic progression of sentinel lymph node was evaluated using a Lumina II imaging system (Caliper Life Sciences, MA, USA). Before imaging, the mice were anesthetized with a 2% isofluorane/air mixture and given a single i.p. dose of 150 mg/kg D-luciferin in normal saline. Bioluminescence imaging was accomplished between 5 and 10 min post-luciferin administration. A photographic image was collected followed by acquisition and overlay of a pseudocolor luminescent image representing the spatial distribution of the detected photons emitted from the active luciferin within the tumor cells.

MR imaging and data analysis

MRI scans were performed with a Bruker PharmaScan 7T/16 scanner equipped with a mouse body volume coil. The animal was placed on an animal bed equipped with circulating warm water to regulate body temperature during magnetic resonance imaging scans. While the animal was under anesthesia, anatomic magnetic resonance imaging was done using a T_2-weighted spin echo sequence with RARE (rapid acquisition with relaxation enhancement) technique. The acquisition parameters are as following: repetition time (TR)/ echo time (TE), 2,000/48.8 ms; 256 ×256 matrix; and a 30 × 30 mm field of view (FOV). Continuous 1 mm thick slices were used to cover the entire tumor region. A magnetic resonance-compatible small animal respiratory gating device was used during the scans. The size of the lymph nodes was determined by measuring the short-axis diameter with T_2-weighted MRI.

DWI data were collected using a standard spin echo sequence with two b-factors (0 and 1,000 s/mm^2) at three orthogonal gradient directions (x, y, z). The acquisition parameters are as follows: bandwidth, 50505.1 Hz; TR/TE, 2750/90 ms; diffusion separation time, 16 ms; diffusion gradient duration, 6 ms; 128 ×128 matrix; and a 30 × 30 mm FOV. A total of three to five 1-mm-thick slices (1-mm gap) were used to cover regions of interest (ROIs). ADC maps were automatically reconstructed for all diffusion-weighted images. For the ADC calculation, an ROI was drawn on the b = 1000 s/mm^2 DW image within each lymph node at the slice in which the largest ROI could be drawn. The ADC map was calculated by fitting the signal of the diffusion weighted images to the Stejskal–Tanner Equation: $S(b) = S_0 * e^{-b*ADC}$ to the data points at 2 b-values: 0 and 1000 mm^2/s, with S_0 and ADC as fit parameters [5].

For SPIO enhanced MRI, 20 μmol of SPIO (0.56 mg/kg in 20 μl Feridex I.V.; Berlex Laboratories, Inc., Wayne, NJ, USA) per extremity was administered locally 6 hours later. The acquisition parameters were as the following: TR/TE, 2000/48ms; FA, 180° FOV, 3×3cm; Matrix, 256×256; NEX, 4.

Histological evaluation

After MR imaging, the popliteal lymph nodes were identified and dissected along with the surrounding tissue and fixed with 4% formalin. The lymph nodes were subsequently embedded in paraffin and the sections were stained with hematoxylin and eosin. Prussian blue iron stain was used to assess the presence and intra-nodal distribution of SPIO particles.

Statistical analysis

Lymph node size and change of ADC were evaluated statistically. Statistical analysis was performed with a two-tail Student's *t*-test. A *p* value less than 0.05 was considered statistically significant.

Results

Establishment of metastatic lymph nodes

In this study, we developed metastatic lymph nodes by hock injection of firefly luciferase expressing 4T1 mouse mammary tumor cells [23]. Similar to footpad inoculation, subcutaneous cell or CFA inoculation in hock region resulted in metastatic or reactive popliteal lymph nodes in all mice. As shown in Fig. 1, positive bioluminescent signal was detectable in the collateral popliteal region at day 21 after cell inoculation, indicating that tumor cells metastasized to the local draining lymph nodes. Due to the tumor cell proliferation within the lymph node, the BLI signal was much stronger at day 28. No positive BLI signal was observed in CFA treated mice at all the time points (data not shown).

CFA enhances antibody production and induces an inflammatory response, primarily at the inoculation site. Consistent with previous studies [24, 25], enlargement of the lymph nodes was recognized at day 7 after either tumor cell inoculation or CFA administration (Fig. 2). From day 7 to day 21, no apparent difference in the size of affected lymph node was observed between tumor cell inoculated group and CFA group. At day 28, the metastatic lymph node showed dramatic size increase as compared to day 21 ($p < 0.01$), while the lymph node volume of CFA injected mice remained virtually unaltered from day 21 to day 28.

ADC map of lymph nodes

At all the time points examined, reactive lymph nodes showed homogeneous signal intensities on both T_2WI and ADC map. At early time points up to day 21, relatively homogeneous signal intensity was observed within the tumor draining LNs on both T_2WI and ADC map. At day 28, 4 out of 5 enlarged metastatic lymph nodes showed homogeneous signal ntensity on the T_2WI. Focal central necrosis was found in 1 lymph node. In contrast, heterogeneous signal distribution of ADC map was found in all 5 TLNs (Fig. 2).

To calculate ADC value of each lymph node, we drew ROI directly on ADC map within each lymph node at the slice in which the largest ROI could be drawn. As shown in Fig. 2d, no difference in the mean ADC of tumor induced and inflammation induced lymph nodes was found at early stages up to 21 days post inoculation. At day 28, ADC of metastatic LNs was $0.41 \pm 0.03 \times 10^{-3}$ mm^2/s, which was significantly higher than that of reactive LNs ($0.34 \pm 0.02 \times 10^{-3}$ mm^2/s, $p < 0.05$).

Alignment of ADC map with HE staining

After aligning the ADC map with the HE staining section, we found that the high value regions on the ADC map correspond to metastatic tumors (Fig. 3). More homogeneous ADC map of reactive lymph nodes corresponds to hyperplastic inflammatory reaction. These results suggest that increased ADC value in tumor metastatic LNs is mainly due to proliferating tumor cells. On the HE staining, we found that metastatic tumors presented lower cellularity than the surrounding lymphatic tissue, which may account for the locally increased ADC value and patchy heterogeneity observed on the ADC maps.

SPIO MRI

Superparamagnetic nanoparticles are phagocytosed by macrophages in the normal lymphoid tissues, where they induce T_2 shortening and decreasing signal intensity [19, 20]. After SPIO administration, normal lymph nodes appear dark on MR images while metastatic nodes remain iso-signal intense. As shown in Fig. 4, at day 21 after cell and CFA inoculation, both tumor metastatic and reactive LNs showed distinct T_2 signal reduction at

the central region after interstitial administration of iron oxide. Metastatic lymph nodes demonstrated faint T_2 signal reduction at subcapsular area. At day 28, metastatic lymph nodes showed heterogeneous signal intensity, indicating uneven distribution of the iron oxide particles within the lymph node. Prussian blue staining also revealed different patterns of iron oxide in reactive and metastatic LNs. Iron oxide was mainly distributed in medullary sinuses. In tumor metastatic LNs, medullary sinuses uptake also contributed to the locally reduced signal intensity. However, proliferating tumor cells showed minimal iron oxide uptake, which corresponds to the region without signal reduction.

Discussion

ADC value has been calculated in different nodal pathologies/conditions. It is convincing that DWI and ADC measurements are effective in differentiating these different nodal pathologies [26–28]. However, the ADCs of normal lymph nodes and those of different nodal pathologies or conditions overlap since DWI highlights both normal and pathologic lymph nodes [29]. In this study, T2WI showed homogeneous signal intensity in both reactive and tumor metastatic LNs. However, heterogeneous signal distribution of ADC map was found only in TLNs. The results suggest that ADC map is more sensitive than T2WI in distinguishing reactive and tumor metastatic LNs. At day 28, ADC of metastatic LNs was significantly higher than that of reactive LNs ($p < 0.05$), which is consistent with previously reported results that metastatic lymph nodes have higher ADC values than benign lymph nodes[14].

Multiple factors such as tissue cellularity, cell membrane permeability, and extracellular matrix composition can affect ADC measurement [5]. Consequently, several groups reported that metastatic lymph nodes have lower ADC values, which may be explained by the histological alterations caused by carcinoma deposits in the nodal micro-architecture consisting of densely packed enlarged cells and an increase of mitotic figures [11, 15]. We found that the high value regions on the ADC map correspond to metastatic tumors, indicating that increased ADC value in tumor metastatic LNs is mainly due to proliferating tumor cells. This finding is further justified by the lower cellularity of the metastatic tumors than the surrounding lymphatic tissue (Fig. 3).

High-quality DWI images is very important for qualitative analysis of ADC value, especially for small animal lymph nodes. Since DWI is very sensitive to motion [30], we chose the popliteal lymph node. Using this model can minimize motion artifacts and consequently increase accuracy of ADC measurement. Moreover, there is only one single popliteal lymph node in the popliteal fossa of the murine rear leg and the anatomic location of the popliteal lymph node is constant, superficial, and easy to identify by palpation. The mean ADC of normal lymph nodes was not evaluated due to the limitations in the spatial resolution of our MR systems. Although the vendor-supplied sequence was improved at our institution, susceptibility artifacts and image distortions along the phase encoding gradient could not be eliminated completely. Consequently, the accurate determination of ADC values in smaller lymph nodes is not feasible.

The measurement of ADC is relatively independent of lesion size if the area of lymph node allows drawing a ROI. DWI requires short scanning time, thus ADC measurement can be acquired as a part of routine MR examination. However, ADC is dependent on many factors which cause variation of tissue diffusivity and regional gradient, such as body temperature, tissue pressure, perfusion rate, or magnetic environment of individual subject [3, 31]. Although we confirmed that increased ADC in metastatic LNs was a result from proliferating tumor cells, the ADC map failed to tell the difference between reactive and metastatic LNs when only small subcapsular metastatic foci are present. Thus, we agree that

normalized ADC, called relative ADC, is necessary for common general application of a certain threshold for differentiating metastatic from nonmetastatic lymph nodes [32].

It has been demonstrated that intravenously administered SPIO decreases signal intensity of normal but not metastatic nodes [33]. Compared with systemic administration, a more selective enhancement of the lymphatic system can be achieved with interstitial MR lymphography. For example, it has been reported that SPIO did not show uptake in lymph nodes after intravenous administration since rapid clearance of the particles by the reticuloendothelial systems of the liver and spleen [34]. For interstitial administration, a whole network of lymphatic vessels is perfused. Thus, a more reliable and even distribution of the contrast agent will be achieved into regional nodes. Moreover, interstitial MR lymphography can vastly decrease the dose of contrast agent and potentially harmful side effects [34, 35].

The major possible pathway underlying is initial interstitial distribution, followed by uptake of SPIOs by draining lymphatic vessels and transport to regional lymph nodes via afferent lymphatic channels and subsequent phagocytosis by macrophages in the lymph nodes [33, 36]. Consequently, we observed that metastatic lymph nodes showed heterogeneous signal intensity, indicating uneven distribution of the iron oxide particles within the lymph node. This can be explained by the fact that proliferating tumor cells have minimal iron oxide uptake.

Conclusion

With apparent metastatic tumor cell proliferation, both diffusion-weighted and SPIO enhanced MRI can distinguish tumor metastatic lymph nodes with reactive lymph nodes. However, both methods have limited value in detecting microscopic tumor metastasis to the draining lymph nodes at the very early stage.

Acknowledgments

This project was supported in part by the Intramural Research Program of the National Institute of Biomedical Imaging and Bioengineering (NIBIB), National Institutes of Health (NIH), and the International Cooperative Program of the National Science Foundation of China (NSFC) (81028009).

References

1. Kim SH, Kim SC, Choi BI, Han MC. Uterine cervical carcinoma: evaluation of pelvic lymph node metastasis with MR imaging. Radiology. 1994; 190:807–11. [PubMed: 8115631]
2. Oyen RH, Van Poppel HP, Ameye FE, et al. Lymph node staging of localized prostatic carcinoma with CT and CT-guided fine-needle aspiration biopsy: prospective study of 285 patients. Radiology. 1994; 190:315–22. [PubMed: 8284375]
3. Lei J, Xue HD, Li Z, Li S, Jin ZY. Possible pathological basis for false diagnoses of lymph nodes by USPIO-enhanced MRI in rabbits. J Magn Reson Imaging. 2010; 31:1428–34. [PubMed: 20512896]
4. King AD, Ahuja AT, Yeung DK, et al. Malignant cervical lymphadenopathy: diagnostic accuracy of diffusion-weighted MR imaging. Radiology. 2007; 245:806–13. [PubMed: 17911539]
5. Klerkx WM, Geldof AA, Heintz AP, et al. Longitudinal 3.0T MRI analysis of changes in lymph node volume and apparent diffusion coefficient in an experimental animal model of metastatic and hyperplastic lymph nodes. J Magn Reson Imaging. 2011; 33:1151–9. [PubMed: 21509874]
6. Lin G, Ho KC, Wang JJ, et al. Detection of lymph node metastasis in cervical and uterine cancers by diffusion-weighted magnetic resonance imaging at 3T. J Magn Reson Imaging. 2008; 28:128–35. [PubMed: 18581404]
7. Le Bihan D. Molecular diffusion, tissue microdynamics and microstructure. NMR Biomed. 1995; 8:375–86. [PubMed: 8739274]

8. Roy C, Bierry G, Matau A, Bazille G, Pasquali R. Value of diffusion-weighted imaging to detect small malignant pelvic lymph nodes at 3 T. Eur Radiol. 2010; 20:1803–11. [PubMed: 20182732]
9. Patterson DM, Padhani AR, Collins DJ. Tecnology insight: water diffusion MRI--a potential new biomarker of response to cancer therapy. Nat Clin Pract Oncol. 2008; 5:220–33. [PubMed: 18301415]
10. Kwee TC, Takahara T, Ochiai R, Nievelstein RA, Luijten PR. Diffusion-weighted whole-body imaging with background body signal suppression (DWIBS): features and potential applications in oncology. Eur Radiol. 2008; 18:1937–52. [PubMed: 18446344]
11. Abdel Razek AA, Soliman NY, Elkhamary S, Alsharaway MK, Tawfik A. Role of diffusion-weighted MR imaging in cervical lymphadenopathy. Eur Radiol. 2006; 16:1468–77. [PubMed: 16557366]
12. Eiber M, Beer AJ, Holzapfel K, et al. Preliminary results for characterization of pelvic lymph nodes in patients with prostate cancer by diffusion-weighted MR-imaging. Invest Radiol. 2010; 45:15–23. [PubMed: 19996762]
13. Sumi M, Sakihama N, Sumi T, et al. Discrimination of metastatic cervical lymph nodes with diffusion-weighted MR imaging in patients with head and neck cancer. AJNR Am J Neuroradiol. 2003; 24:1627–34. [PubMed: 13679283]
14. Sumi M, Van Cauteren M, Nakamura T. MR microimaging of benign and malignant nodes in the neck. AJR Am J Roentgenol. 2006; 186:749–57. [PubMed: 16498102]
15. Eiber M, Beer AJ, Holzapfel K, et al. Preliminary results for characterization of pelvic lymph nodes in patients with prostate cancer by diffusion-weighted MR-imaging. Invest Radiol. 2010; 45:15–23. [PubMed: 19996762]
16. Anzai Y, Piccoli CW, Outwater EK, et al. Evaluation of neck and body metastases to nodes with ferumoxtran 10-enhanced MR imaging: phase III safety and efficacy study. Radiology. 2003; 228:777–88. [PubMed: 12954896]
17. Harisinghani MG, Barentsz J, Hahn PF, et al. Noninvasive detection of clinically occult lymph-node metastases in prostate cancer. N Engl J Med. 2003; 348:2491–9. [PubMed: 12815134]
18. Pultrum BB, van der Jagt EJ, van Westreenen HL, et al. Detection of lymph node metastases with ultrasmall superparamagnetic iron oxide (USPIO)-enhanced magnetic resonance imaging in oesophageal cancer: a feasibility study. Cancer Imaging. 2009; 9:19–28. [PubMed: 19414293]
19. Yu MK, Park J, Jon S. Targeting strategies for multifunctional nanoparticles in cancer imaging and therapy. Theranostics. 2012; 2:3–44. [PubMed: 22272217]
20. Huang J, Zhang X, Wang L, Yang L, Mao H. Improving the magnetic resonance imaging contrast and detection methods with engineered magnetic nanoparticles. Theranostics. 2012; 2:86–102. [PubMed: 22272222]
21. Lim SW, Kim HW, Jun HY, et al. TCL-SPION-enhanced MRI for the detection of lymph node metastasis in murine experimental model. Acad Radiol. 2011; 18:504–11. [PubMed: 21216633]
22. Vassallo P, Matei C, Heston WD, McLachlan SJ, Koutcher JA, Castellino RA. AMI-227-enhanced MR lymphography: usefulness for differentiating reactive from tumor-bearing lymph nodes. Radiology. 1994; 193:501–6. [PubMed: 7972768]
23. Aslakson CJ, Miller FR. Selective events in the metastatic process defined by analysis of the sequential dissemination of subpopulations of a mouse mammary tumor. Cancer Res. 1992; 52:1399–405. [PubMed: 1540948]
24. Krzystyniak K, Kozlowska E, Desjardins R, et al. Different T-cell activation by streptozotocin and Freund's adjuvant in popliteal lymph node (PLN). Int J Immunopharmacol. 1995; 17:189–96. [PubMed: 7558513]
25. Zhang F, Niu G, Lin X, et al. Imaging tumor-induced sentinel lymph node lymphangiogenesis with LyP-1 peptide. Amino Acids. 201110.1007/s00726-011-0976-1
26. de Bondt RB, Hoeberigs MC, Nelemans PJ, et al. Diagnostic accuracy and additional value of diffusion-weighted imaging for discrimination of malignant cervical lymph nodes in head and neck squamous cell carcinoma. Neuroradiology. 2009; 51:183–92. [PubMed: 19137282]
27. Holzapfel K, Duetsch S, Fauser C, Eiber M, Rummeny EJ, Gaa J. Value of diffusion-weighted MR imaging in the differentiation between benign and malignant cervical lymph nodes. Eur J Radiol. 2009; 72:381–7. [PubMed: 18995981]

28. Vandecaveye V, De Keyzer F, Vander Poorten V, et al. Head and neck squamous cell carcinoma: value of diffusion-weighted MR imaging for nodal staging. Radiology. 2009; 251:134–46. [PubMed: 19251938]

29. Kwee TC, Takahara T, Ochiai R, et al. Complementary roles of whole-body diffusion-weighted MRI and ^{18}F-FDG PET: the state of the art and potential applications. J Nucl Med. 2010; 51:1549–58. [PubMed: 20847177]

30. Dietrich O, Heiland S, Benner T, Sartor K. Reducing motion artefacts in diffusion-weighted MRI of the brain: efficacy of navigator echo correction and pulse triggering. Neuroradiology. 2000; 42:85–91. [PubMed: 10663480]

31. Unger JB, Ivy JJ, Ramaswamy MR, Charrier A, Connor P. Whole-body [^{18}F]fluoro-2-deoxyglucose positron emission tomography scan staging prior to planned radical hysterectomy and pelvic lymphadenectomy. Int J Gynecol Cancer. 2005; 15:1060–4. [PubMed: 16343182]

32. Kim JK, Kim KA, Park BW, Kim N, Cho KS. Feasibility of diffusion-weighted imaging in the differentiation of metastatic from nonmetastatic lymph nodes: early experience. J Magn Reson Imaging. 2008; 28:714–9. [PubMed: 18777531]

33. Weissleder R, Elizondo G, Wittenberg J, Lee AS, Josephson L, Brady TJ. Ultrasmall superparamagnetic iron oxide: an intravenous contrast agent for assessing lymph nodes with MR imaging. Radiology. 1990; 175:494–8. [PubMed: 2326475]

34. Weissleder R, Elizondo G, Josephson L, et al. Experimental lymph node metastases: enhanced detection with MR lymphography. Radiology. 1989; 171:835–9. [PubMed: 2717761]

35. Herborn CU, Lauenstein TC, Vogt FM, Lauffer RB, Debatin JF, Ruehm SG. Interstitial MR lymphography with MS-325: characterization of normal and tumor-invaded lymph nodes in a rabbit model. AJR Am J Roentgenol. 2002; 179:1567–72. [PubMed: 12438057]

36. Oghiso Y, Matsuoka O. Time-dependent changes of microscopic localization of intravenously administered colloidal carbon particles in mouse lymph nodes. J Toxicol Sci. 1983; 8:291–300. [PubMed: 6663659]

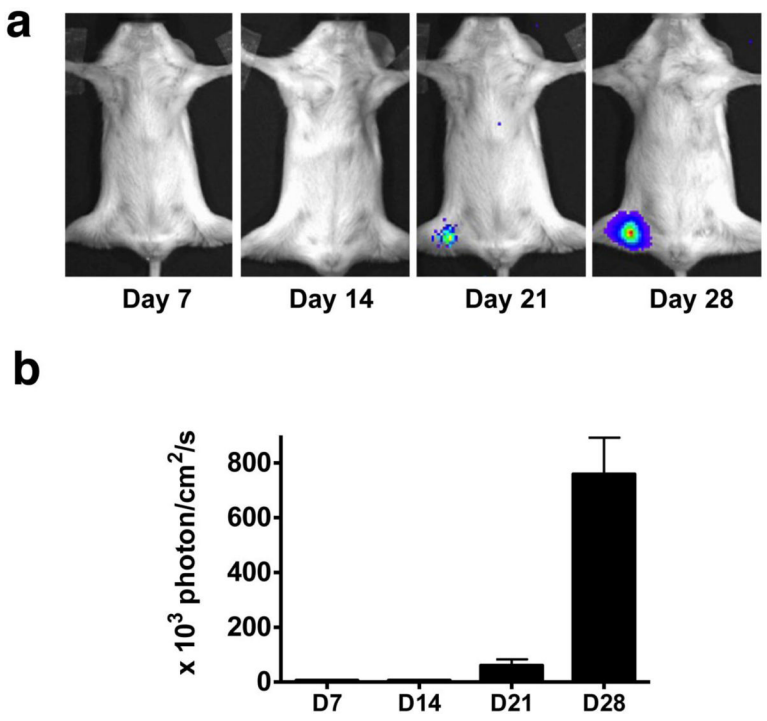

Figure 1.
(a) Bioluminescence imaging (BLI) of tumor metastasis to tumor draining lymph nodes. **(b)** Quantification of tumor burden based on BLI.

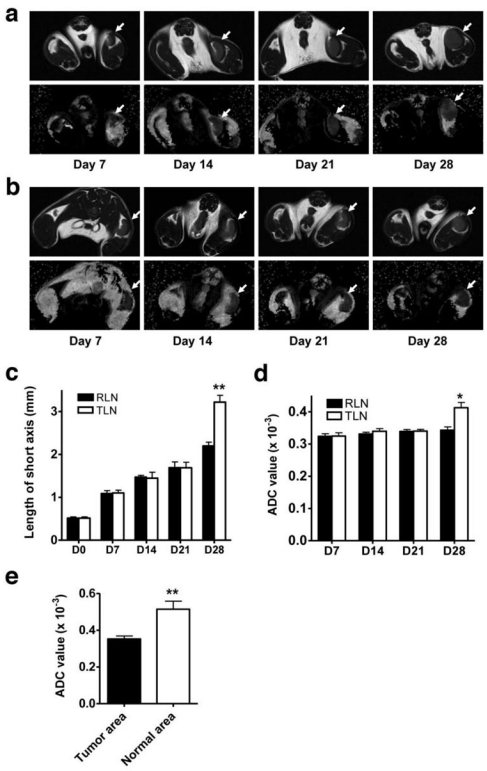

Figure 2.

T_2 weighted MRI (upper panel) and ADC map (lower panel) of tumor draining lymph nodes **(a)** and reactive lymph nodes **(b)** at different time points after tumor cell or CFA inoculation. **(c)** Size of tumor draining and reactive lymph nodes measured through the short axis. **(d)** Average ADC value of tumor draining and reactive lymph nodes. **(E)** ADC value of lymphatic area and metastatic tumor area within tumor metastatic lymph nodes at day 28 after inoculation. * $p < 0.05$; ** $p < 0.01$.

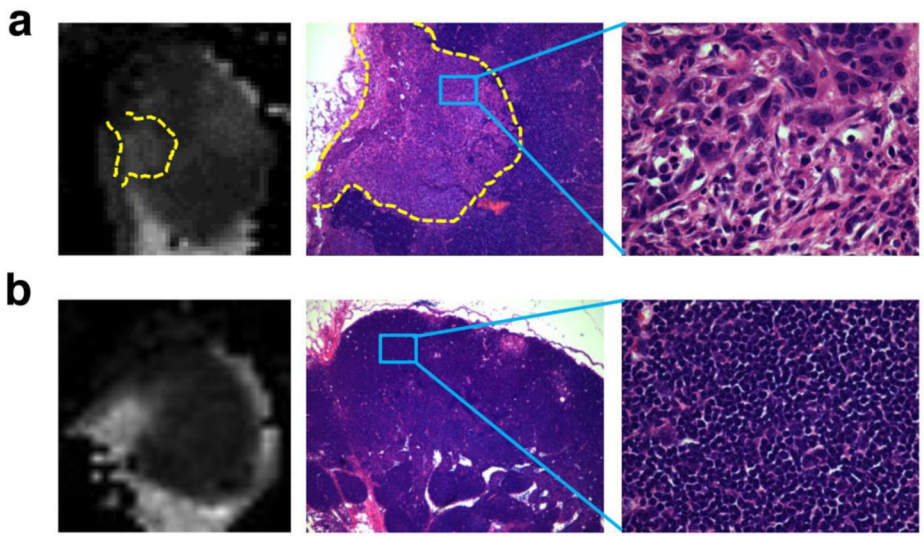

Figure 3.
(a) ADC map and HE staining of tumor metastatic lymph nodes at day 28 after inoculation. Tumor cell proliferation on HE staining (200 x magnification) correlated with the heterogeneity of ADC map. **(b)** ADC map and HE staining of reactive lymph nodes.

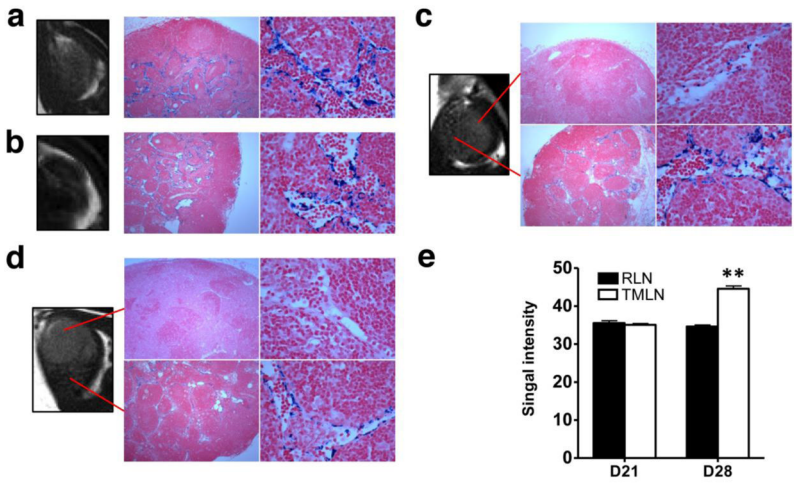

Figure 4.

T_2 weighted MRI and Prussian blue staining (200 magnification) of reactive lymph nodes **(a & b)** and tumor draining lymph nodes **(c & d)** at day 21 **(a & c)** and day 28 **(b & d)** after inoculation. Photomicrograph of histologic specimen was obtained after injection of superparamagnetic iron oxide. The iron-laden cells of the medullary sinusoids were stained blue by the Prussian blue reaction and sharply outline the pink counterstained cortex and medullary cords. Compared with hyperplastic lymphatic tissue, proliferating tumor cells showed much less iron oxide uptake and T2 reduction. **(e)** Quantification of T_2 signal intensity of lymph nodes.

Table 1

Imaging protocol for the mice, in days after tumor cell inoculation and CFA injection

Group	7 d	14 d	21 d	28 d
Tumor cell inoculation (n=15)				
BLI	15	15	15	10
DWI-MRI (n=5)	5	5	5	5*
SPIO MRI (n=5)			5*	
SPIO MRI (n=5)				5*
CFA injection (n=15)				
BLI	15	15	15	10
DWI-MRI (n=5)	5	5	5	5*
SPIO MRI (n=5)			5*	
SPIO MRI (n=5)				5*

MRI was performed immediately after BLI imaging.

*, lymph nodes sampling